



Development of a frictionally damped boring bar for chatter suppression in boring process

Sajad Hayati¹ · Mehdi Shahrokhi² · Ali Hedayati¹

Received: 6 August 2020 / Accepted: 8 February 2021 / Published online: 24 February 2021
 © The Author(s), under exclusive licence to Springer-Verlag London Ltd. part of Springer Nature 2021

Abstract

A novel boring bar was developed for chatter reduction of machining processes. By proposing an internal frictional damping structure, additional energy dissipation during bending vibrations was imposed to the boring bar. The structure consisted of some pins longitudinally press-fitted inside the boring bar. This structure resisted against bending of the boring bar during machining processes. After introducing the structure, an analytical model was presented to determine the amount of energy dissipated by the damper. Using the analytical model and finite element modeling (FEM), the most effective configuration was obtained for the proposed frictional damper structure. After determining the best configuration, a damped boring bar specimen was fabricated for experimental comparison with a regular boring bar. The modal and cutting tests were performed on the specimens. The modal test revealed a significant increase in the structural damping of the boring bar. The cutting tests were performed at different depths of cut and different spindle speeds, and the process was investigated through sound analysis and surface finish observation. Experimental comparisons indicated the higher performance of the proposed tool.

Keywords Boring · Chatter suppression · Frictional damper

Nomenclature

A_c	Sound amplitude at the chatter frequency
$A(i), A(t)$	The sound amplitude of the i^{th} sample or at time (t)
A_{rms}	Root mean square of the sound amplitude in the time domain
a	Depth of cut (mm)
D_i	The slip on the contact surfaces of the i^{th} pin (Analytical model)
d_i	The absolute value of relative displacement on the i^{th} contact node (FEM)

E	The equal elasticity modulus for all parts
E_b, E_i	Elasticity modulus for tool body and i^{th} pin individually
e	Contact surfaces interference
F	The total lateral force applied to the tooltip
F_b, F_i	The portion of F applied to the tool body and the i^{th} pin
G_{xx}, G_{yy}	Direct FRFs at the tool tip in x and y directions (regular/damped tools)
G_{xy}, G_{yx}	Cross FRFs at the tool tip in x and y directions (regular/damped tools)
I	The overall moment of inertia of the tool body and pins
I_b, I_i	The moments of inertia for the tool body and pins individually
L	Free length of the tool
N_c	Number of contact nodes in the FEM
n	Number of inserted pins
P_{ave}	The average contact pressure for all pins
P_i	Contact pressure on the i^{th} pin
R	Radius of the circle where center of pins are located on
$R_{\text{max}}, R_{\text{min}}$	Maximum and minimum radii of the tool body
Δ	Lateral deflection at the tooltip

✉ Sajad Hayati
 s.hayati@kut.ac.ir

Mehdi Shahrokhi
 alico.1990@yahoo.com

Ali Hedayati
 hedayatiali1372@gmail.com

¹ Department of Mechanical Engineering, Faculty of Energy, Kermanshah University of Technology (KUT), Kermanshah, Iran

² Mechanical Unit, Kermanshah Petrochemical Industries Company (KPIC), Kermanshah, Iran

δ_b, δ_i	Displacement of tool body and i^{th} pin on contact surfaces
$\varepsilon_b, \varepsilon_i$	Strain of tool body and i^{th} pin on contact surfaces
θ	The angular variable around each pin ($0 \leq \theta < 2\pi$)
ζ_1	Damping ratio of the (regular/damped) tool related to the first resonance
μ, μ_i	Friction constant of the pins or the i^{th} pin
σ_i	Normal contact pressure on the i^{th} contact node of the FEM
τ_i	Tangential frictional stress on the i^{th} contact node of the FEM
ϕ	Constant angular distance between two neighbor pins ($\phi = 2\pi/n$)
ϕ_i	Angular distance between positive direction of x -axis on neutral axis of the tool and the i^{th} pin
Ω	Spindle speed (rpm)
ω_1	The first natural frequency of the (regular/damped) tool in lateral directions (Hz)
ω_c	Chatter frequency (Hz)
ω_s	Sampling frequency of digital sound recording (Hz)

1 Introduction

Chattering is defined as self-excited vibration of machining tools causing chip removal limitations in machining processes. Chatter vibrations reduce the productivity of machining processes causing a poor surface finish and tool wear. Studies on chatter vibrations have led to a variety of methods to prevent chattering in different machining processes such as techniques found in the state of the art reviews [1–4].

The proposed strategies are applied to the machining parameters or to the machine tool structure. In the first category, one or more parameters of the machining process are altered to avoid chattering. Yang et al. [5] applied multiple time-varying parameters including the spindle speed and rake angle for chatter suppression in the turning process. According to their results, varying multiple parameters by time was more effective than varying a single parameter. The optimal variable helix tool geometry proposed by Yusoff and Sims [6] led to a fivefold increase in the chatter stability of the milling process in practice. A similar study was conducted on variable pitch and helix milling tools [7] to improve the milling process stability. An automatic cutting feed adjustment system is also designed for chatter suppression in turning process integrating the operational characteristics of cutting force to shorten the machining time and maintain the workpiece quality [8].

As another chatter suppression strategy, the time-varying spindle speed has been used in the turning and milling

processes [9, 10]. Yamato et al. [11] proposed a method for selecting the optimal amplitude and frequency of sinusoidal spindle speed variation to achieve the highest stability limit. Wang et al. [12] proposed multi-harmonic spindle speed variation with a phase factor for chatter suppression in the milling process. In addition, Petrakov [13] developed technologies for chatter suppression via controlling the cutting speed and the CNC machine drive of the forming motion. Another strategy based on mode coupling chatter prediction is utilized to determine the correct stable machining setup including machining parameters, robot pose, travel direction, and workpiece setup for chatter avoidance in robotic machining processes [14]. Despite widespread applications of spindle speed variation methods for chatter suppression, they might be harmful imposing a large momentum into the rotating parts of the machine tool while decreasing the tool lifetime [15, 16].

Strategies applied to the machine tool structures are categorized into three major classes, namely, active, semi-active, and passive strategies. Active structural control methods are based on the feedback control concept in which a direct force is applied to the structure. In this case, the actuation is applied to the tools, fixtures, bearings, or any other parts of the machining process, even the workpiece. For instance, Sallese et al. developed active fixtures to stabilize the milling process by generating counteracting vibrations [17, 18]. Different types of actuators have been used for structural control such as biaxial inertial actuators used by Munoa et al. for vibration absorption of a milling machine [19].

In addition, piezoelectric stack actuators applying direct force to the machining structure were experimentally applied for active chatter suppression in milling [20]. The piezoelectric actuators were also applied for chatter suppression in milling processes based on the model predictive control [21] and robust control [22] strategies. Moradian et al. [23] applied a piezoelectric actuator at the end of a boring bar for chatter suppression through adaptive sliding mode control approach. Wan et al. [24] used an active spindle system with a non-contact electromagnetic actuator for chatter suppression in the milling process.

In semi-active methods, mechanical properties of the structure such as the stiffness and damping are varied by the feedback control depending on vibration conditions. For example, Alammari et al. [25] investigated shifting the natural frequency of the tool for chatter suppression through fluid level control and a mass at the end of a boring bar. Hayati et al. [26] proposed another strategy by varying the mass and stiffness of a slender boring bar with a mechanical system. Adaptive tuned mass dampers are among the semi-active tools used for chatter reduction [27]. Piezoelectrics are other semi-active structural control tools widely used for chatter reduction. Wang et al. [28] changed the stiffness of a milling tool for chatter reduction via piezoelectric stack actuators. An asymmetric stiffness control system using piezoelectric actuators

was also proposed by Li et al. [29]. Moreover, piezoelectric patches were used by Tang et al. [30] to increase the stability limit of the boring process. Magneto-rheological fluids have also been used for semi-active chatter suppression of boring bars modulating the stiffness or increasing the damping ratio [31, 32].

Despite the effectiveness of structural active and semi-active vibration control strategies, they are usually complicated and need additional expenses and advanced maintenance by skilled staff.

Despite a lower performance, there has been a great interest in simple passive methods in industrial applications. For example, improvement of boring tools damping and chatter suppression were attempted by Ema and Marui [33] using impact dampers. Miguélez et al. [34] applied passive vibration absorption strategies to the machining processes using vibration absorbers such as tuned mass dampers to improve the stability of the boring processes. Yang et al. [35] installed multiple vibration absorbers on a machine tool structure. Mechanical parameters of the vibration absorbers such as the mass, stiffness, damping, and location must be accurately tuned according to the tool properties and cutting conditions. Optimization methods such as classical optimization method are commonly used for this purpose as applied by Rubio et al. [36] to tune an absorber for chatter reduction in the boring process. A receptance coupling-based method was also presented by Bansal and Law [37] to optimally tune and place a tuned vibration absorber on slender boring bars. In a similar study, Yadav et al. proposed the chatter-resistant damped boring bars using a receptance coupling approach [38].

Passive vibration absorbers are accurately tuned via different tuning methods for various types of tools and machine tools, but they are just effective in a limited frequency bound. In contrast, energy dissipation methods are not limited to a certain frequency bound.

Piezoelectric materials with passive shunt circuits are used for passive energy dissipation of vibrations in both boring and turning processes [39, 40]. Chattering can also be reduced by submerging the milling tool in a viscous fluid [41]. Portentos et al. [42] made a comparison between the dynamic responses of two columns of milling machines made of classic metal-working and metal foam sandwiches to show the effect of using different materials in damping of the machine tools.

Frictional dampers are among the simplest passive tools for energy dissipation without any need for tuning. Marui et al. [43] first used frictional dampers for chatter prevention in cutting tools. The proposed mechanism consisted of a plate inserted into a rectangular hole at the overhanging shank of the cutting tool to increase the damping capacity through friction between the inner wall of the hole and the surface of the inserted plate. Furthermore, a multi-fingered hollow cylinder frictional damper embedded inside an axial borehole in a milling tool was proposed for chatter reduction [44, 45]. The

centrifugal force generated via spindle rotation pressed the fingers against the inner surface of the tool leading to energy dissipation during bending vibration. This plan was further improved by adding a core inside the fingers leading to a higher pressure because of the press-fitting of the parts instead of rotation [46, 47].

In this study, a new form of frictional damper structure is proposed inside the boring bar to improve its structural damping. The structure consists of some pins longitudinally press fitted inside the boring bar. Figure 1 illustrates the assembling of the proposed boring bar parts for a damped boring bar with two pins. As seen, the longitudinal holes with a diameter of $2r-2e$ are created inside the boring bar, and the pins with a diameter of $2r$ are inserted inside the holes, where e is a small number representing the surface interference causing a pressure between the contact surfaces and resistance of this structure against bending vibration.

As a full-fledged form of the previously developed frictional dampers, the proposed plan makes maximum use of the internal space of the tool body to achieve the highest possible damping effect. Unlike the damper developed by Marui et al. [43], the damper proposed in this study causes no damage to the tool surface. Consequently, its application does not decrease the tool stiffness as reported in [43–45]. The damper mechanism relies on the press fitting pressure; thus, it can be used in both rotating and non-rotating tools unlike the dampers proposed in [44, 45]. Furthermore, application of the proposed damper is not limited to circular solid sections unlike some previously developed dampers [44–47]. It can be also used for vibration reduction in any solid or hollow beam shaped and even flat structures. A comprehensive methodology and instruction are also used for the design and application of such frictional dampers.

A novel modeling and optimization scheme is presented to maximize the damper effect. The effect of the proposed structure on the improved damping of the boring bar is evaluated by calculating the dissipated energy through an analytical modeling process. An analytical model is also used to achieve an optimal structural configuration with the maximum effect.

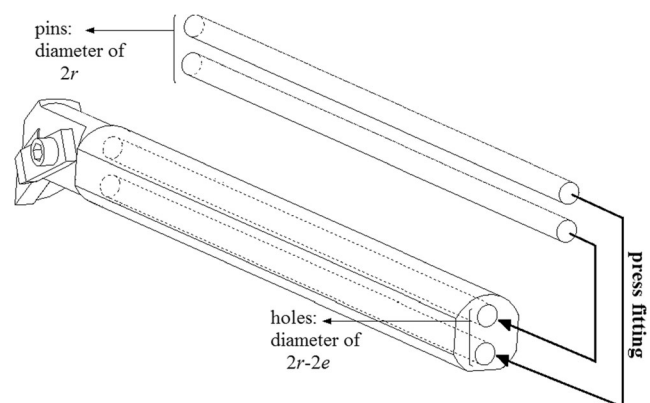


Fig. 1 Assembling of the damped boring bar parts

A specimen of the damped boring bar is then fabricated with the optimum configuration. The modal and cutting tests are applied to the developed tool and a similar ordinary tool. The results revealed a significant improvement in the machining performance by the proposed structure.

2 Modeling

In this section, the performance mechanism of the damper structure is investigated, and a mathematical model is presented for calculating the dissipated energy. The model is then used for optimizing the damper configuration.

2.1 Damper performance mechanism

The damper mechanism can be deduced from Fig. 2 illustrating the front- and side-section views of a cylindrical tool body with two axially inserted pins (Pin1 and Pin2). The lateral surfaces of the pins and internal surfaces of the tool holes are in contact. As seen, for every pin, the vertical distance between the neutral axis (N.A.) of the pin and that of the tool body (N.A.) equals \bar{y}_i .

This difference in the location of neutral axes leads to different tension/compression strain behaviors of the contacted surfaces. The difference in the strain of the contacted surfaces in turn leads to a sliding movement between the surfaces. The pins are press-fitted inside the tool body pressing the contact surfaces. As a result, frictional forces are imposed on the sliding surfaces leading to frictional energy dissipation inside the tool body.

The entire system is considered a beam which is free at $z=0$ and clamped at the other end ($z=L$) to understand the sliding behavior of the contact surfaces between the tool body and pins. Based on the literature on the boring chatter force, a total lateral force (F) of 200 N is exerted by the workpiece to the free end of the beam [48].

The tool body alone can be considered a separated beam with the same boundary conditions imposed by its own portion of force (F_b). The i^{th} pin can also be considered another beam with its own portion of force (F_i). The deflection of all beams (Δ) is considered as follows [46]:

$$\begin{aligned} \Delta &= \frac{F}{EI} \left(\frac{-z^3 + 3zL^2 - 2L^3}{6} \right) \\ &= \frac{F_b}{E_b I_b} \left(\frac{-z^3 + 3zL^2 - 2L^3}{6} \right) \\ &= \frac{F_i}{E_i I_i} \left(\frac{-z^3 + 3zL^2 - 2L^3}{6} \right) \end{aligned} \tag{1}$$

where E_b , I_b , E_i , and I_i represent the elasticity modulus and moment of inertia for the tool body and the i^{th} pin, respectively. The force equilibrium is expressed as follows:

$$F = F_b + \sum_{i=1}^n F_i \tag{2}$$

Obviously:

$$EI = E_b I_b + \sum_{i=1}^n E_i I_i \tag{3}$$

where n represents the total number of inserted pins. The following equation can be concluded from Eqs.1, 2, and 3.

$$\frac{F}{E_b I_b + \sum_{i=1}^n E_i I_i} = \frac{F_b}{E_b I_b} = \frac{F_i}{E_i I_i} \tag{4}$$

The strain of each component on the contact line can be then obtained as follows. For the i^{th} pin, $r_i \sin \theta$ is the normal distance between the contact line and N.A.i where $0 \leq \theta < 2\pi$ is the angular variable around each pin (Fig. 2). Therefore, the strain on the external surface of each pin with respect to z is obtained as follows:

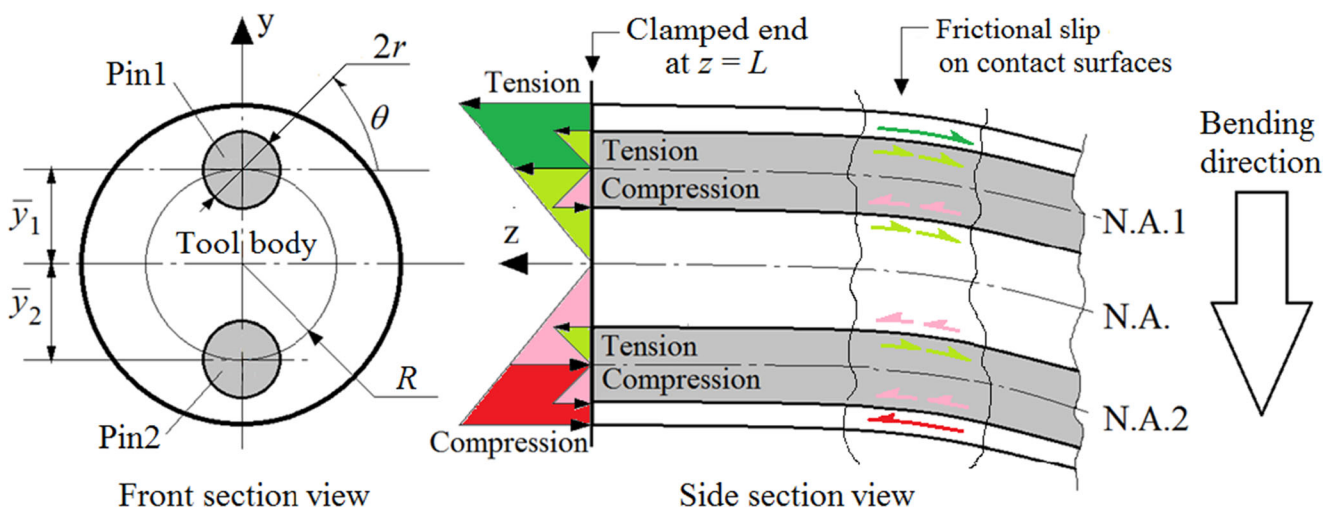


Fig. 2 The performance mechanism of the proposed damper

$$\varepsilon_i = \frac{F_i z}{E_i I_i} r_i \sin\theta \tag{5}$$

Similarly, the normal distance between the contact line and N.A. is equal to $\bar{y}_i + r_i \sin\theta$, and the strain on the contact surfaces of the tool body is obtained as follows:

$$\varepsilon_b = \frac{F_b z}{E_b I_b} (\bar{y}_i + r_i \sin\theta) \tag{6}$$

The displacement on the contact surfaces for the tool body (δ_b) and pins (δ_i) is then achieved as follows:

$$\delta_i = \int_z^L \varepsilon_i dz = \int_z^L \frac{F_i z}{E_i I_i} r_i \sin\theta dz = \frac{F_i r_i \sin\theta}{2E_i I_i} (L^2 - z^2) \tag{7}$$

$$\delta_b = \int_z^L \varepsilon_b dz = \int_z^L \frac{F_b z}{E_b I_b} (\bar{y}_i + r_i \sin\theta) dz = \frac{F_b (\bar{y}_i + r_i \sin\theta)}{2E_b I_b} (L^2 - z^2) \tag{8}$$

The slip on the contact surfaces of the i^{th} pin (D_i) can now be obtained as the absolute difference of displacements. According to Eq. 4, the displacements are calculated as follows:

$$D_i = |\delta_b - \delta_i| = \frac{F |\bar{y}_i|}{2EI} (L^2 - z^2) \tag{9}$$

The amount of dissipated energy can be calculated by multiplying the friction force by the slip value. Assuming constant distribution of the contact pressure on each pin, the friction force on the i^{th} pin can be calculated by multiplying the contact pressure (P_i) on the surface area by the friction constant (μ_i) of that pin. The differential frictional work (dW_i) is obtained on a surface element ($dA=r_i dz d\theta$) of the i^{th} pin as follows:

$$dW_i = \mu_i P_i \frac{F |\bar{y}_i|}{2EI} (L^2 - z^2) r_i dz d\theta \tag{10}$$

For the contact surfaces of the i^{th} pin, the amount of work can be calculated by integrating dW_i over the contact area.

$$W_i = \int_0^{2\pi} \int_0^L \mu_i P_i \frac{F |\bar{y}_i|}{2EI} (L^2 - z^2) r_i dz d\theta = \frac{2\pi L^3 \mu_i r_i P_i F |\bar{y}_i|}{3EI} \tag{11}$$

The total dissipated energy (W_t) is eventually obtained by adding all frictional works for all pins:

$$W_t = \sum_{i=1}^n W_i = \frac{2\pi L^3 F}{3EI} \sum_{i=1}^n \mu_i r_i P_i |\bar{y}_i| \tag{12}$$

Maximizing this equation maximizes the damper effect. As seen, the parameters like F , E , and I are not dependent on the damper configuration. It seems that an increase in F causes a

growth in the damper effect, but the parameter F represents the machining force imposed on the tooltip from the workspace and is dependent on operating conditions. Moreover, this machining force is the main cause of vibration, and its increase is not desirable. A decrease in the parameters E and I also seems to be beneficial for improving the damper effect. However, it should be noted that a decrease in E and I causes a reduction in the stiffness leading to higher vibrations.

The parameter L indicating the length of pins should be maximized, but the maximum length is limited by the tool length and geometry. The parameter μ_i (the friction coefficient of the i^{th} pin contact surface) is equal for all pins represented by μ dealing with steel-steel contact friction coefficient. To improve the damper effect, the friction coefficient can be increased through surface operations. However, such operations are not applied because of press-fitting limitations.

An increase in the parameters r_i , n , and \bar{y}_i specifying the damper structure configuration improves the damping effect (Eq. 12), but the contact pressures must also be computed for a reliable evaluation. Changing the damper configuration affects the contact pressure on each pin (P_i). The pressure on the pins is also dependent on the interference (e) and mechanical properties of the involved bodies. Obviously, an increase in E and e leads to an increase in P_i . However, an excessive increase in the interference value causes difficulties in the press-fitting operation, plastic deformation of bodies, and preventing slip on the contact surfaces. Thus, a constant interference value of $5\mu\text{m}$ was considered for all pins [47].

To achieve the damping effect, the pin centers are not supposed to be on the centerline of the tool body (Eq. 12); therefore, there is not any analytical method to determine the contact pressure on the pins. However, considering pins of equal radii ($r_i=r$) with a symmetric arrangement around the axis of the tool, a same pressure will be actually exerted on the pins. As shown in Fig. 2, the pins are arranged in a circular pattern around the tool axis with a radius of R . An average contact pressure of P_{ave} obtained from the finite element method (FEM) is applied on all pins.

According to the above discussions and Eq. 12, an objective function representing the damper performance can be achieved with respect to the damper effective parameters.

$$W_o = r P_{\text{ave}} \sum_{i=1}^n |\bar{y}_i| \tag{13}$$

The above equation is obtained for a symmetrically arranged damper structure with equal-length pins and an equal friction coefficient for the contact surfaces with an average contact pressure (P_{ave}). Instead of Eq. 12, Eq. 13 can be used as an objective function to maximize the damper effect.

2.2 Finite element modeling

In this section, a finite element model is presented for the damped tool structure. This model is first used as the complementary part of the analytical model for determining the contact pressure between the tool body and pins. It is then used as another criterion for maximizing the damper effect. To develop a finite element model, a real boring tool is considered to apply the damper mechanism. Figure 3 displays the dimensions of the studied boring bar and the related plain diamond-shaped insert in millimeters. As seen, the side surfaces are perpendicular, and the insert nose radius is 0.4 mm with -3° axial rake angle. The size of the pins is also chosen according to the standard pins available in the market. As seen, the cross-section area of the tool body is not completely symmetric.

A 3D model was imported to the ANSYS modeling environment for numerical analysis. A solid element with 20 nodes (solid95) was used to mesh the volumes, and steel material properties were used for both pins and the tool body ($E=210$ GPa, $\nu=0.3$, and $\rho=7800$ kg/m³). Hex dominant and Hex mesh styles were used for the tool body and pins, respectively. For contact surfaces between the pins and the tool body, a 3D surface-to-surface contact was defined using the penalty method to eliminate any surface penetration. In each contact, the pin was considered the contact surface, and the tool body was taken as the target. The CONTA174 contact elements with 8 nodes and TARGE170 were respectively used to model the contact and target surfaces of flexible bodies. The sliding behavior of the contact surfaces was modeled with Coulomb friction assumptions. A constant friction coefficient of $\mu=0.15$ is considered for all steel-steel contact surfaces [44, 47].

A convergence analysis process was performed based on the calculation of the average contact pressure to find a proper number of elements for the problem. The average contact pressure was obtained over the contact surfaces as follows:

$$P_{ave} = \frac{\sum_{i=1}^{N_c} \sigma_i}{N_c} \quad (14)$$

where σ_i indicates the normal contact pressure on the i^{th} contact node and N_c is the number of contact nodes.

In the convergence analysis process, the damped tool with two internal pins was modeled, and the average contact pressure was calculated for different numbers of elements. Figure 4 shows the average pressure as a function of the number of elements. According to the results of convergence analysis, the number of elements for all finite element models is higher than 25,000 elements in this study.

Given the reliability of the finite element model in computing P_{ave} , Eqs. 12 and 13 can be used to calculate the dissipated energy and evaluate the damper performance with different configurations.

Instead of Eq. 12, the finite element model can be individually used to compute the total dissipated energy (W_t) [44]. The total frictional work can be obtained using the contact frictional stress and relative displacements on the contact nodes:

$$W_t = \frac{\sum_{i=1}^{N_c} \tau_i d_i}{N_c} \times 2\pi r L n \quad (15)$$

where τ_i represents the tangential frictional stress on the i^{th} contact node, d_i the absolute value of relative displacement on the i^{th} contact node, and $2\pi r L$ shows the contact surface of each pin that is multiplied by the number of pins (n) to obtain the total contact surface. To perform this evaluation, a lateral force of 200 N was applied to the tooltip in the FEM.

3 Damper configuration optimization

Various damper configurations were investigated using Eqs. 12 and 13 and the FEM to find a configuration that

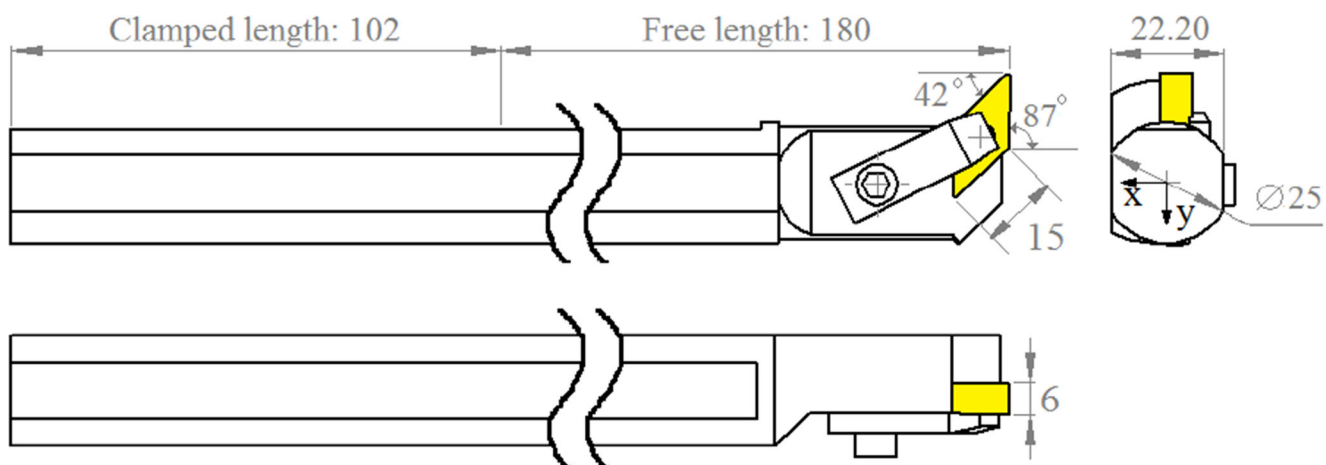
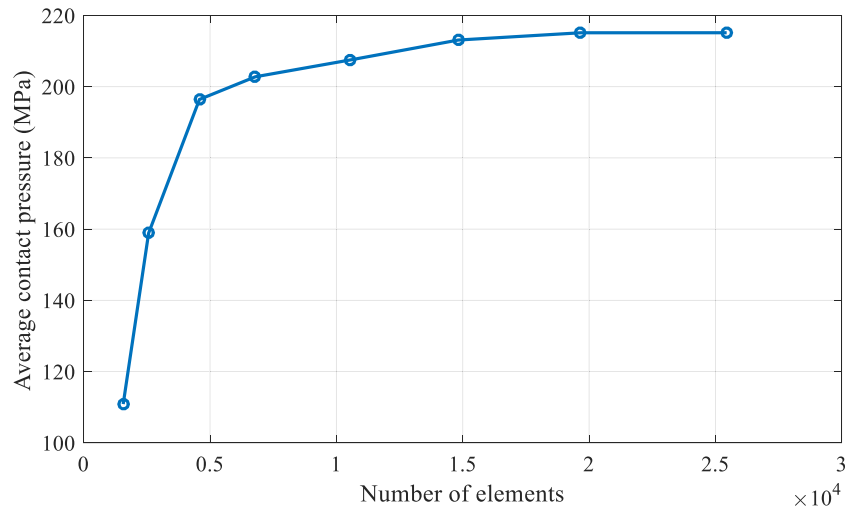


Fig. 3 The geometry and dimensions of the investigated boring bar

Fig. 4 Convergence analysis of the finite element model (FEM)



maximizes the damper effect. Figure 5 shows the general view of the cross-section of a boring bar with n internal pins. The pin centers are assumed to be located on a circle with a radius of R concentric with the tool body at C . There is a constant angle (ϕ) between the radius of this circle meeting the centers of neighbor pins where $\phi = 2\pi/n$. The related radius meeting the center of the i^{th} pin also makes an angle of ϕ_i with the positive direction of the x -axis. Therefore, the effective parameter $\sum_{i=1}^n |\bar{y}_i|$ can be obtained as follows:

$$\sum_{i=1}^n |\bar{y}_i| = R \sum_{i=1}^n |\sin(\phi_i)| = R \sum_{i=1}^n |\sin(\phi_1 + (i-1)\phi)| \quad (16)$$

Therefore, an increase in R may cause an increase in $\sum_{i=1}^n |\bar{y}_i|$ leading to an increase in the damping effect, but its effect on the contact pressure is still unclear. Consulting a manufacturing expert, some feasibility constraints were defined for the damped

tool configuration. To reduce the manufacturing costs, standard pins with integer diameters must be used. Furthermore, pins with diameters less than 4 mm are not supposed to be used because of potential buckling during the press-fitting process. The pin diameter also must be at least 3 mm smaller than the minimum radius of the tool body, $R_{\min}=11.1$ mm (Fig. 3). These constraints are stated as follows:

$$4 \leq 2r \leq (11.1 - 3) \text{ mm, and } 2r \text{ is an integer} \quad (17)$$

Moreover, the distance between the pin surfaces inside the tool body must not be less than 3 mm. As seen in Fig. 5, this constraint can be expressed as follows:

$$2R\sin(\phi/2) - 2r \geq 3 \text{ mm} \quad (18)$$

Fig. 5 Positions of the inserted pins rather than their neighbors and the tool body

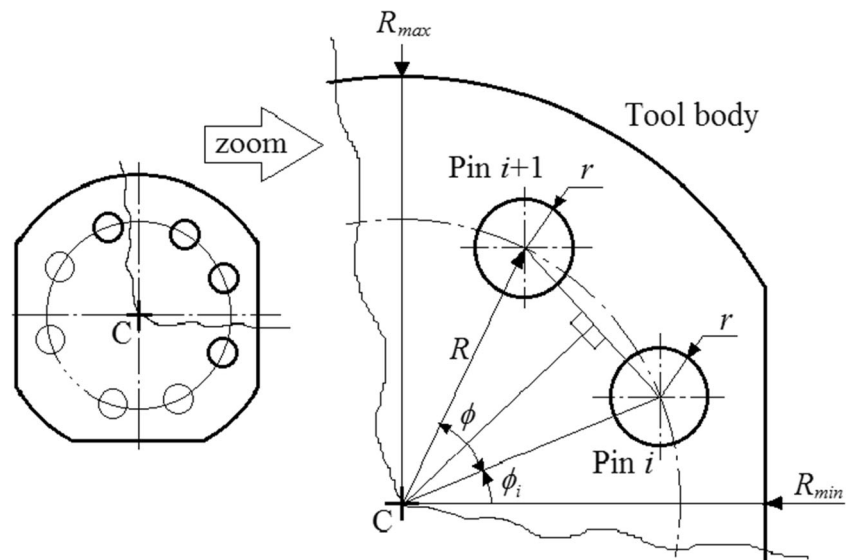


Table 1 All possible configurations for the damped tool with the related performance indices

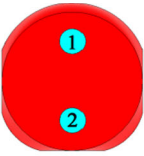
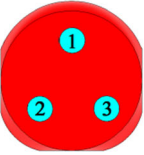
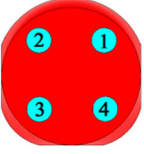
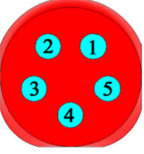
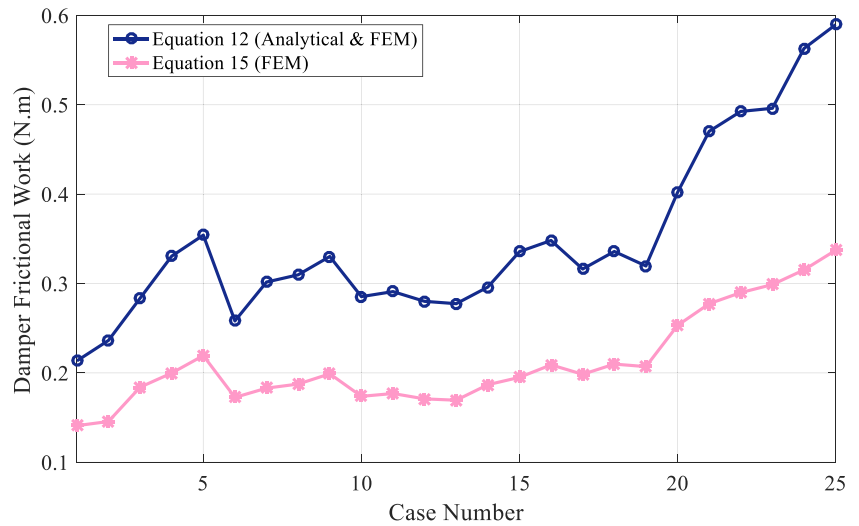
Pins arrangement	Case No.	r (mm)	R (mm)	$\sum_{i=1}^n \bar{y}_i $	P_{ave} (MPa)	W_o	W_t (N.m)	
							Eq.12	Eq. 15
	1	2	3.5	7	288.41	4037.74	0.2134	0.1409
	2	2	4	8	279.36	4469.76	0.2363	0.1456
	3	2	5	10	268.17	5363.44	0.2835	0.1840
	4	2	6	12	260.59	6254.16	0.3306	0.1998
	5	2	6.5	13	257.67	6699.42	0.3541	0.2193
	6	2.5	4	8	244.14	4882.80	0.2581	0.1725
	7	2.5	5	10	228.27	5706.75	0.3016	0.1829
	8	2.5	5.5	11	213.09	5859.975	0.3097	0.1875
	9	2.5	6	12	208.24	6247.20	0.3302	0.1989
	10	3	5	10	179.89	5396.72	0.2853	0.1737
	11	3	5.5	11	166.77	5503.41	0.2909	0.1769
	12	3.5	5	10	151.34	5296.9	0.2800	0.1709
	13	2	4.5	9	291.61	5248.98	0.2774	0.1694
	14	2	5	10	279.97	5599.40	0.2960	0.1868
	15	2	6	12	264.59	6350.16	0.3356	0.1950
	16	2.5	5	10	263.43	6585.75	0.3481	0.2089
	17	2.5	5.5	11	217.54	5982.35	0.3162	0.1984
	18	2.5	6	12	211.78	6353.41	0.3358	0.2098
	19	3	5.5	11	183.25	6047.25	0.3196	0.2070
	20	2	5	14.14	268.82	7602.23	0.4018	0.2531
	21	2	6	16.97	262.11	8896.01	0.4702	0.2773
	22	2	6.5	18.38	253.46	9317.19	0.4925	0.2898
	23	2.5	6	16.97	221.21	9384.83	0.4960	0.2988
	24	2	6	19.42	274.17	10648.76	0.5629	0.3152
	25	2	6.5	21.04	265.02	11152.04	0.5895	0.3371

Fig. 6 Damper dissipated energy from Eq. 12 (analytical and FEM) and Eq. 15 (FEM)



That is simplified as follows:

$$R \sin(\pi/n) \geq r + 1.5 \tag{19}$$

As another feasibility constraint, the normal distance between the pin surfaces and the tool body must not be less than 3 mm. Given the non-circular cross-section of the tool body, the average radius was taken as the limit that can be stated as follows:

$$R + r + 3 \leq \left(\frac{R_{max} + R_{min}}{2} \right) \tag{20}$$

where R_{max} =12.5 mm and the above-mentioned constraint is simplified as follows:

$$R + r \leq 8.8 \approx 8.5 \text{ mm} \tag{21}$$

All possible configurations of the damped tool with their performance indices are listed in Table 1 assuming the constraints. The performance indices are related to the amount of dissipated energy including the objective function (W_o) from Eq. 13 and the total frictional work (W_f) from Eqs. 12 and 15.

According to the results, an increase in R and r causes a decrease in P_{ave} , but the damper performance is improved. This can be attributed to the direct increasing effect of the parameter r on the contact surfaces and also the effect of the parameter R on $\sum_{i=1}^n |\bar{y}_i|$ (Eq. 16). As the number of inserted pins increases, growth in $\sum_{i=1}^n |\bar{y}_i|$ and P_{ave} values leads to a better damping effect. The most effective possible configuration, giving the highest performance, is the 25th damper.

For a better comparison, these results are also displayed in Fig. 6. Taking the results of Eq. 12 as the reference, the

Table 2 The effect of interference variation on tool properties

Results		e (μm)			
		5	10	15	20
P_{ave} (MPa)		221.21	402.83	406.45	411.60
W_f (N.m)	Load: 100 N	0.1139	0.1073	0.1066	0.1032
	Load: 200 N	0.2988	0.2817	0.2792	0.2714
	Load: 300 N	0.4782	0.4511	0.4481	0.4341
	Load: 400 N	0.7012	0.6610	0.6551	0.6368
ω_1 (Hz)		886.2	887.4	884.0	881.3
$\text{Max}(G_{yy})$ (m/N)	Load: 100 N	8.75×10^{-6}	8.86×10^{-6}	9.01×10^{-6}	9.23×10^{-6}
	Load: 200 N	7.38×10^{-6}	7.45×10^{-6}	7.59×10^{-6}	7.76×10^{-6}
	Load: 300 N	6.26×10^{-6}	6.33×10^{-6}	6.44×10^{-6}	6.53×10^{-6}
	Load: 400 N	5.49×10^{-6}	5.55×10^{-6}	5.65×10^{-6}	5.73×10^{-6}

Table 3 Finding the optimum interference value

Results		e (μm)			
		6	7	8	9
P_{ave} (MPa)		258.34	292.43	330.11	364.75
W_f (N.m)	Load: 100 N	0.1138	0.1141	0.1129	0.1101
	Load: 200 N	0.2990	0.2992	0.2961	0.2892
	Load: 300 N	0.4785	0.4791	0.4738	0.4633
	Load: 400 N	0.7017	0.7021	0.6948	0.6786
ω_1 (Hz)		887.2	887.7	888.1	887.6
$\text{Max}(G_{yy})$ (m/N)	Load: 100 N	8.68×10^{-6}	8.65×10^{-6}	8.66×10^{-6}	8.73×10^{-6}
	Load: 200 N	7.36×10^{-6}	7.34×10^{-6}	7.35×10^{-6}	7.41×10^{-6}
	Load: 300 N	6.22×10^{-6}	6.18×10^{-6}	6.20×10^{-6}	6.31×10^{-6}
	Load: 400 N	5.46×10^{-6}	5.42×10^{-6}	5.44×10^{-6}	5.53×10^{-6}

relative error at low pin numbers is about 25% and increases up to 50% at higher pin numbers.

The error increases with increasing the number of contact surfaces due to increase in nonlinearity. Furthermore, full slip was considered ($F_f = \mu N$) for all contact surfaces in the analytical model, whereas the amount of slip varies from zero at the clamped end to its maximum value at the free end of the pins (Eq. 9). Therefore, pre-slip occurrence is assured [46] where the induced frictional force is less than that in full slip. The pre-slip condition is taken into account in the FEM; thus, lower but more realistic values are expected. In addition, in reality and FEM, the contact pressure is not constant over the

contact surfaces, while it is assumed to be constant in the analytical approach. The FEM also has the capability to model much more complicated geometries. Despite significant differences, similar trends confirm a reliable optimization.

Having an experimental evaluation of the proposed damped tool, a real specimen was fabricated. It was decided to choose the case 23 to simplify the fabrication process.

The interference value (e) is a key parameter in the design of the damped tool. Obviously, the contact pressure increases with an increase in the interference value. However, it can also lead to stiction of the contact surfaces causing a decrease in the dissipated energy. An FEM analytical study was performed to

Fig. 7 Damped tool fabrication and the appearance of the damped tool in comparison with the regular tool

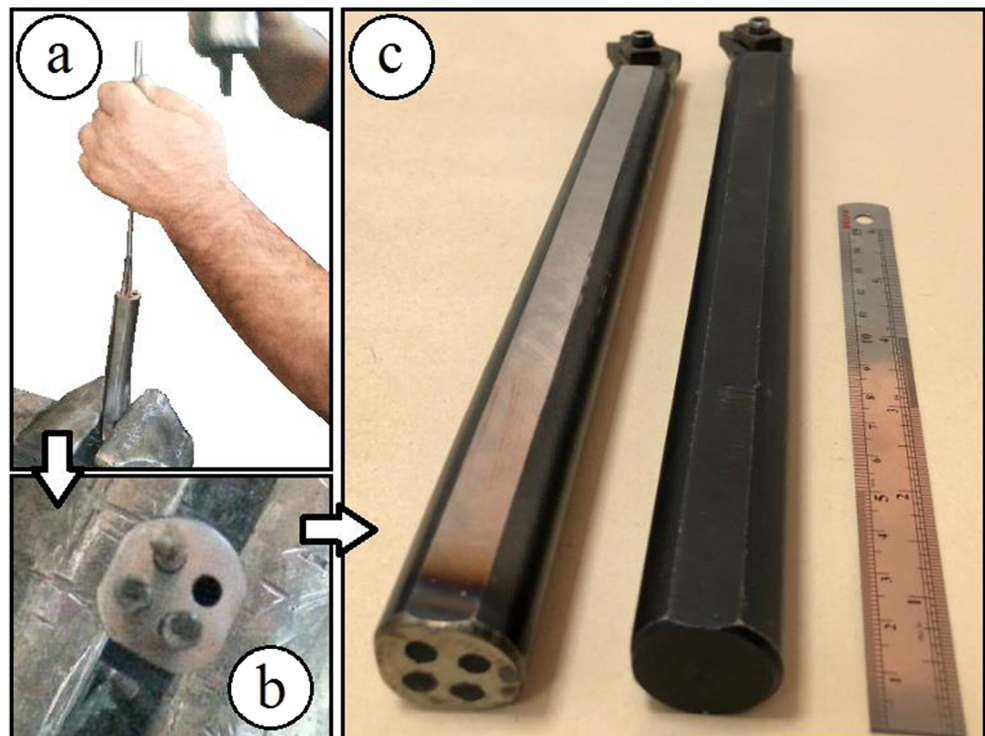
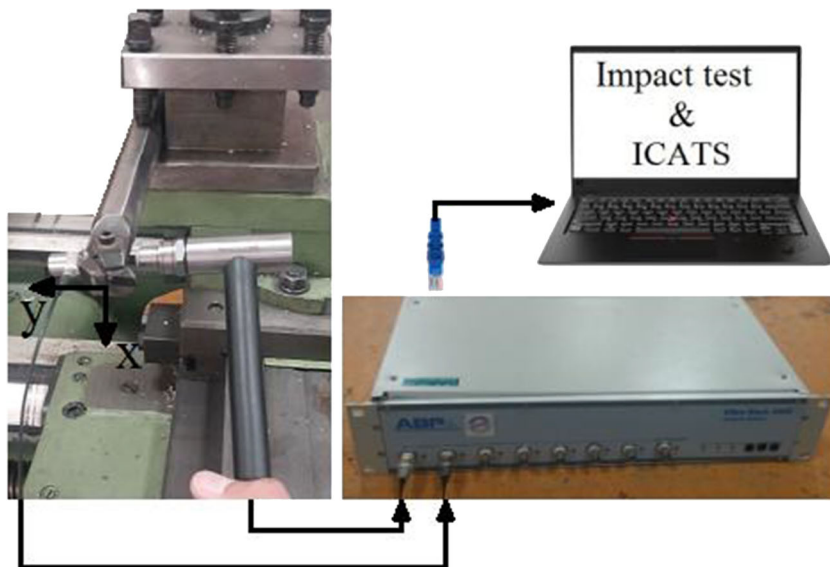


Fig. 8 The modal test setup and related directions



find an optimal interference value. As seen below, the FEM has capability to give various results which are more beneficial for investigation of the plan.

Because of feasibility considerations, the maximum interference value equals 20 μm . Furthermore, the highest achievable accuracy of the used CNC spark machine was about 10 μm . Therefore, the feasible interference values of 5, 10, 15, and 20 μm were considered.

The FEM was used to obtain the important properties of the damped tool. An increase in the interference may lead to plastic stress; thus, the tool body was modeled as a bilinear material with $\sigma_{\text{yield}}=400\text{ MPa}$, $\varepsilon_{\text{yield}}=0.0019$, $\sigma_U=550\text{ MPa}$, and $\varepsilon_U=0.0730$.

The first solution was a static solution to obtain P_{ave} , and the second one was to obtain W_t (Eq. 15) under 100, 200, and 300 and 400 N static loads at the tooltip to cover the problem nonlinearity. The third one was a harmonic solution to obtain the frequency response function at the tooltip in the x-direction and the first natural frequency. The harmonic solution was performed applying the harmonic loads of 100, 200, 300, and 400 N in the frequency range of 850 to 900 Hz with a

step size of 0.1 Hz to cover the first lateral natural frequency. The resulting displacement amplitude in the y-direction was then divided by the load amplitude to obtain the corresponding frequency response function (G_{yy}). The maximum amplitude of this frequency response function ($\text{Max}(|G_{yy}|)$) was then extracted as the most important index of the damper performance that must be minimized. The results are shown in Table 2.

The damping ratio for the harmonic solution was initially taken equal to 0.02 with respect to the former experiments on similar structures. However, after modal test of the regular boring bar, it was modified to 0.0146.

Table 2 reveals that the best interference value might happen for $e=6, 7, 8,$ and $9\ \mu\text{m}$, and the related results are presented in Table 3.

As seen, the best damper performance is obtained at $e=7\ \mu\text{m}$. It is concluded that the optimum interference value is achieved when $P_{\text{ave}} \approx 0.75\sigma_{\text{yield}}$. However, the difference is insignificant and avoiding the plastic contact stress seems to be enough. Therefore, a conservative interference value of 5 μm was used in the fabrication process.

Table 4 The modal test results for experimentally obtained FRFs

FRF	Regular tool properties				Damped tool properties			
	ω_1 (Hz)	ζ_1	$\min(\text{Re}(G))$	K_m (MN/m)	ω_1 (Hz)	ζ_1	$\min(\text{Re}(G))$	K_m (MN/m)
$G_{yy}: X/F_x $	881.7	0.0143	-5.56×10^{-6}	3.5742	890.5	0.0196	-3.98×10^{-6}	3.5873
$G_{yx}: Y/F_x $	880.1	0.0153	-0.84×10^{-6}	-0.8226	889.5	0.0199	-0.69×10^{-6}	-1.2939
$G_{xx}: Y/F_y $	910.9	0.0149	-5.01×10^{-6}	3.8454	923.3	0.0197	-3.58×10^{-6}	3.8579
$G_{xy}: X/F_y $	909.5	0.0149	-0.73×10^{-6}	-0.8226	922.2	0.0213	-0.56×10^{-6}	-1.2939
Average:	895.5	0.0149	-	-	906.4	0.0201	-	-

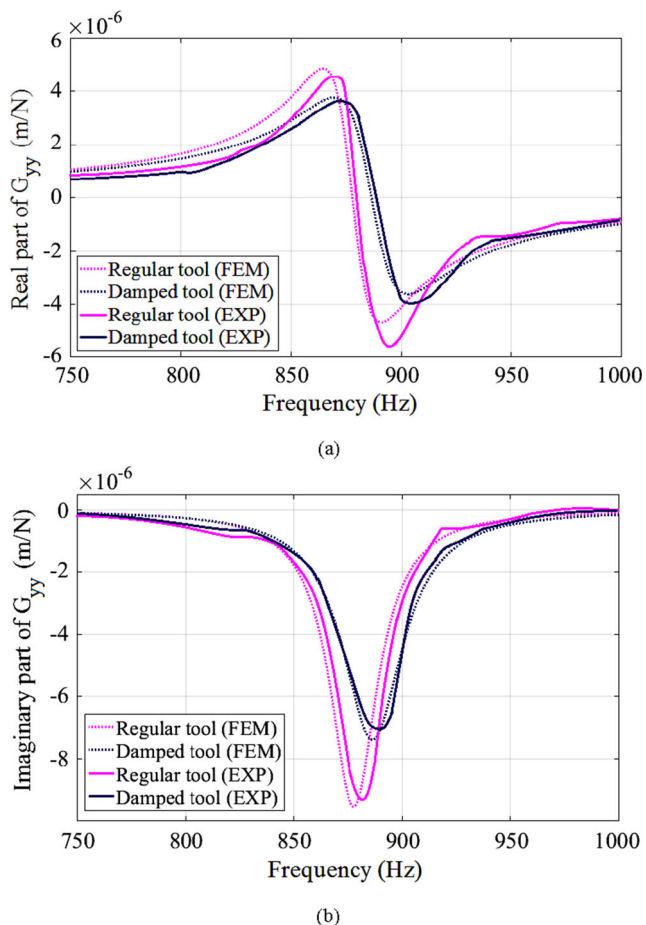


Fig. 9 G_{yy} FRF plots for the damped and regular tools in comparison with FEM results around ω_1 , (a) real part and (b) imaginary part

4 Experiments

A specimen of the damped boring tool was fabricated for experimental investigations. The modal and cutting tests were

performed to evaluate the performance of the developed tool in comparison with a regular tool.

4.1 Damped tool fabrication

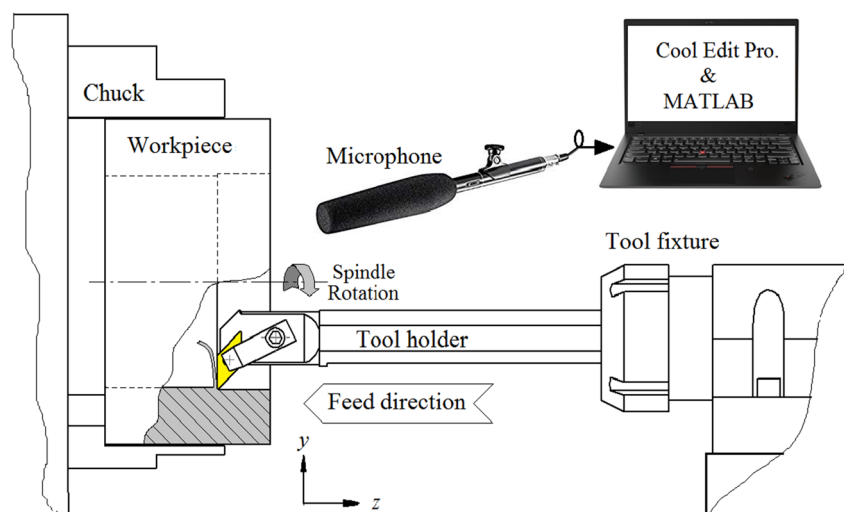
An ordinary boring bar with dimensions shown in Fig. 3 was transformed into the proposed frictionally damped tool as shown in Fig. 7. Using an EDM CNC spark machine, 4 axial holes were created with a depth of 235 mm and a diameter of 4.99 mm around a circle with a radius of 6 mm, and 4 pins with a length of 235 mm and a diameter of 5 mm were press-fitted inside the axial holes. After razing the end of the tool, the frictionally damped boring bar was ready to be used in the experiments.

4.2 Modal testing

The modal testing was applied to the both specimens to compare their dynamic behaviors. The modal test setup in Fig. 8 consists of an impulse hammer (AU02), an axially sensitive piezoelectric accelerometer (AP2037-100), a VibroRack1000 analyzer, and a laptop with Impact Test and ICATS software. The accelerometer data is twice integrated to achieve the displacement at the tooltip. This setup was used to gain the admittance (displacement/force) frequency response functions (FRFs) in 4 different situations, namely, G_{xx} obtained when the hammer impact was imposed in the x-direction and the sensor was installed in the x-direction, G_{yx} with the hammer impact in the y-direction and the sensor in the x-direction, G_{yy} with the hammer impact in the y-direction and the sensor in the y-direction, and G_{xy} with the hammer impact in the x-direction and the sensor in the y-direction.

Figure 8 shows the x- and y-directions. Both tools are installed on a traditional lathe fixture with a free length of 180 mm.

Fig. 10 Cutting test conditions and components including the tool, workpiece, microphone, and laptop



Using the Impact Test software, the data from the impact hammer and sensor were collected in the analyzer and then transferred to the laptop to be analyzed with the help of ICATS. The FRFs were then obtained and the dynamic parameters were extracted.

Chattering usually occurs at the first natural frequency of the tool (ω_1), and the associated damping ratio (ζ_1) significantly affects the chatter stability level [49]. The most important vibration factors and the first resonance modal stiffness at

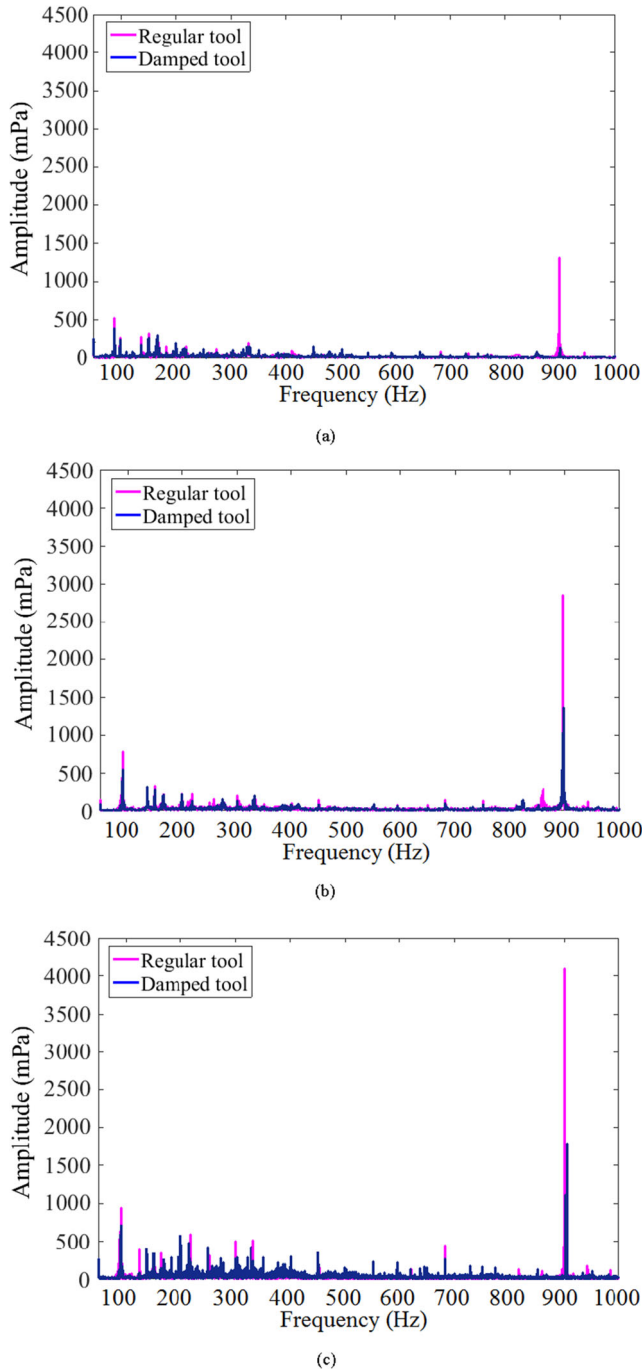


Fig. 11 The FFTs from the process sounds at $\Omega=5500$ rpm, (a) $a=0.5$, (b) $a=1$, and (c) $a=1.5$ mm

the tooltip (K_m) are shown in Table 4. In addition, minimum part of each FRF is presented that is inversely related to the minimum stable depth of cut. These values were extracted through line fitting to the FRFs using ICATS.

Table 4 shows a significant improvement in the damping ratio of the proposed tool in comparison with the regular tool. The average increase in the damping ratio is 34.9% with a maximum of 43% and a minimum of 30%. A higher damping ratio leads to an increase in the chatter stability level [50]. Moreover, a slight increase is observed in the natural frequency (average: 1.2%, maximum: 1.4%, minimum: 1%) due to stiction at the contacts leading to 2.4% increase in the average static stiffness. The insignificant stiffness growth shows that the proposed damper imposes no stiffness reduction as reported in the literature.

For instance, Fig. 9 shows the real and imaginary parts of G_{yy} around ω_1 . The FRFs resulted from FEM are compared with those obtained from the modal test. The results show a good agreement between the FEM and experiments. The damping ratio for FEM of both tools is taken equal to 0.0146 similar to the regular tool. As seen, the damped tool has a lower displacement than the regular tool in most frequencies.

Using the experimental FRFs, the stability lobe diagrams (SLDs) of the boring process can be analytically extracted for both the damped and regular tools [49, 50]. SLDs specifying the limit of stable depth of cut at every spindle speed are the most important criteria to evaluate the tool performance. The minimum stable depth of cut depends on minimum value of real part of the oriented FRF. As seen in Table 4, the minimum stable depth of cut may be increased by more than 35% using the developed damped boring bar.

4.3 Cutting tests

For further evaluation of the effect of the developed structure on the boring stability, cutting tests were performed on the damped and regular tools. Chatter detection by sound analysis was also used to show the effect of the proposed tool on the machining process at different spindle speeds. The resulting surface finishes are also presented.

Both tools with carbide inserts were installed on an MTC-250 CNC lathe machine tool to perform the boring operation inside some AISI 1040 steel bushes with an internal diameter of 93.5 mm. The boring process was performed at $\Omega=4500$, 5000, 5500, 6000, and 6500 rpm at 0.5, 1, and 1.5 mm depths of cut (a).

The machining process sound was recorded by a microphone at a distance of 5 cm from the tooltip as a 16-bit mono wav file with a sampling frequency of 44.1 kHz. The sound was recorded using Cool Edit Pro. software. The microphone tip was coated by a soft cover to reduce the effect of chip throwing impacts on the recorded sound. Figure 10 shows

Table 5 The indices obtained from the cutting test sound analysis

Ω (rpm)	a (mm)	Indices							
		Regular tool				Damped tool			
		A_{rms}	ω_c (Hz)	A_c	Stability condition	A_{rms}	ω_c (Hz)	A_c	Stability condition
4500	0.5	982.70	879.70	290.71	Stable	823.41	887.72	91.43	Stable
	1	1998.86	890.46	1665.04	Marginal	1020.65	891.45	796.11	Stable
	1.5	2308.51	887.81	2384.15	Chatter	1253.82	890.55	1195.12	Marginal
5000	0.5	1893.44	886.40	1419.52	Chatter	1035.34	893.60	215.09	Marginal
	1	2523.17	893.11	2912.00	Chatter	2206.01	891.68	2127.14	Chatter
	1.5	2735.75	890.84	3825.39	Chatter	2564.58	895.51	2595.95	Chatter
5500	0.5	1620.90	888.95	1331.02	Marginal	1240.19	899.19	137.93	Stable
	1	2206.21	897.52	2843.28	Chatter	1576.98	898.22	1402.99	Marginal
	1.5	2623.00	901.09	4100.42	Chatter	1890.75	901.80	1811.11	Chatter
6000	0.5	1368.81	893.86	513.64	Stable	1024.32	894.65	193.45	Stable
	1	2381.46	888.16	2446.07	Chatter	2246.50	890.52	2242.28	Chatter
	1.5	2690.15	890.66	2932.68	Chatter	2516.26	891.71	2519.83	Chatter
6500	0.5	735.66	887.54	177.94	Stable	544.17	888.69	65.20	Stable
	1	1515.18	887.33	603.23	Marginal	992.64	889.70	316.13	Stable
	1.5	1989.85	887.25	888.37	Marginal	1185.12	891.53	474.42	Stable

the cutting test setup including tools installed on the lathe machine with a free length of 180 mm, a microphone (ATR6550 Audio-Technica) connected to a laptop, and the workpiece.

The process sound amplitudes in millipascal (mPa) were recorded in the time domain and then analyzed in the frequency domain using fast Fourier transform (FFT) analysis. The minimum length of each recorded sound was 5 s, and the data was processed in MATLAB. Figure 11 displays the sound FFTs at a spindle speed of 5500 rpm and $a=0.5, 1, \text{ and } 1.5$ mm. As seen, the proposed tool decreases the process sound amplitude and thereby induced vibrations.

According to the FFTs, the damped tool causes a decrease in the sound amplitude around the first natural frequency of the tools. Therefore, the probability of chatter occurrence was decreased in all the tests.

Similar results were obtained at $\Omega = 4500, 5000, 6000, \text{ and } 6500$ rpm, and all the test results are summarized as related indices in Table 5 including the root mean square of the sound amplitude in the time domain (A_{rms}) representing the sound intensity between 0 and t_{max} , chatter frequency (ω_c), and the sound amplitude at the chatter frequency (A_c). The parameter A_{rms} is obtained with respect to the sound amplitude in the time domain ($A(t)$) as follows:

$$A_{\text{rms}} = \sqrt{\frac{1}{t_{\text{max}}} \int_0^{t_{\text{max}}} (A(t))^2 dt} = \sqrt{\frac{1}{t_{\text{max}}} \sum_{i=1}^{t_{\text{max}} \omega_s} \frac{(A(i))^2}{\omega_s}} \quad (22)$$

where ω_s represents the sampling frequency for a digital audio signal, $t_{\text{max}} \omega_s$ the total number of samples, $1/\omega_s$ the sampling time, and $A(i)$ is the amplitude of the i^{th} sample. The sound amplitude increases suddenly when chatter vibration occurs at the maximum stable depth of cut as shown by Quintana et al. [51]. The process stability conditions are classified as stable, marginal, or chatter with respect to the A_c and A_{rms} values in Table 5.

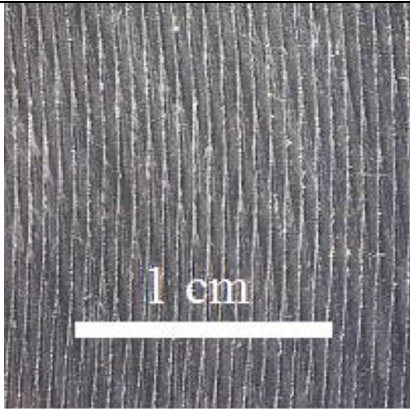
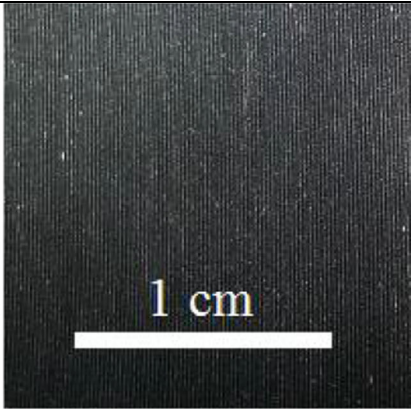
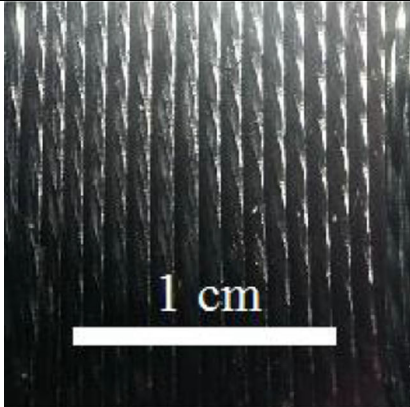
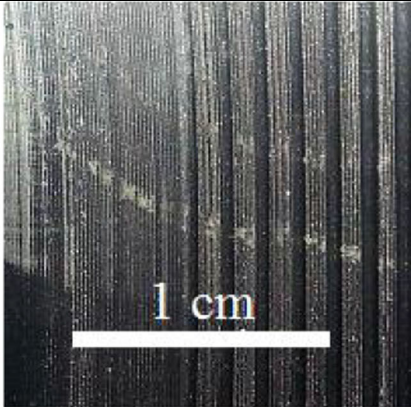
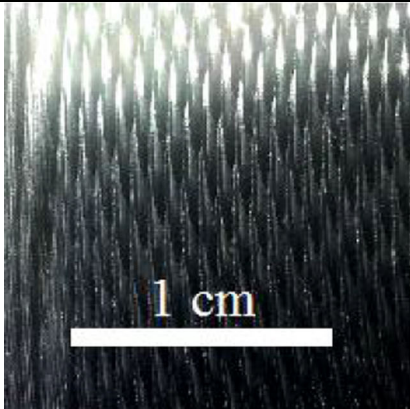
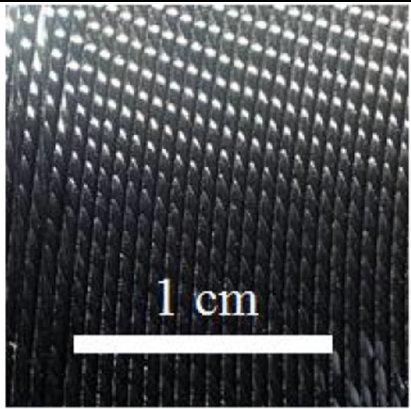
Table 6 lists the resulting surface finishes for the cutting tests in 5500 rpm. Chatter vibrations cause a poor surface finish leaving clearly visible scratches over the workpiece. Therefore, surface finish observation is another method for chatter detection.

The results in Table 6 are consistent with the sound analysis results. In other words, the proposed damped tool was able to improve the machining stability and quality in all cases.

5 Conclusion

A boring bar with an internal frictional damper was proposed to reduce chatter vibrations of boring bars. This simple frictional damper consisted of some pins axially press fitted inside the boring bar. This structure caused resistance and energy dissipation during the bending vibration. A comprehensive analysis was performed for the design and application of such dampers including the simplified analytical model, finite

Table 6 The surface finishes after cutting tests in 5500 rpm

a (mm)	Surface finish	
	Regular tool	Damped tool
0.5		
1		
1.5		

element modeling (FEM), experimental modal analysis, and cutting tests.

First, an analytical model was developed to calculate the amount of dissipated energy in the damper structure. The model was further assisted using an FEM. To find the most effective damper configuration, the amount of dissipated energy was calculated for all possible cases by

the analytical models taking all limitations and constraints into account. According to the optimization trend, the largest possible number of pins must be press-fitted inside the tool to achieve the best damper configuration among the possible cases. Moreover, the pins diameter must be as large as possible with the maximum possible distance from the tool axis.

An FEM analysis was also performed to find the best interference value between the contact surfaces assuming the likelihood of plastic deformation. The best interference value was that generating 75% of the yield stress as the contact pressure.

Eventually, a damped tool with the optimum configuration was fabricated with 4 inner pins with a diameter of 5 mm. The pins were press-fitted inside 4 holes with a diameter of 4.99 mm arranged around the central axis of the tool on a circle with a radius of 6 mm.

The modal and cutting tests were applied to the damped tool and a regular tool. In similar studies performed on a milling tool with a circular frictional damper [46, 47], 25% increase in the damping ratio and 1% increase in the modal stiffness were observed. Using the new frictional dampers proposed in this study, the internal space was fully utilized to maximize the damping effect. The modal test results showed 34.9% increase in the damping ratio and 2.4% increase in stiffness of the damped tool in comparison with the regular tool. In addition, unlike some other frictional dampers developed in [43–45], no damage was imposed to the tool structure and stiffness.

Having FRFs of both tools from the modal test, it was concluded that the limit of stable depth of cut for the damped tool was higher than that of the regular tool.

The cutting tests were then applied to the both tools to investigate the effect of the proposed structure on the machining stability. The boring process was performed with both tools under similar conditions at spindle speeds of 4500, 5000, 5500, 6000, and 6500 rpm at 0.5, 1, and 1.5 mm depths of cut. Each cutting process was evaluated using the sound FFT analysis and workpiece surface finish observation.

The experimental results were in good agreement with each other confirming that the proposed damped tool was able to improve the machining process stability. The developed tool was able to remove a higher amount of chip from the workpiece in a certain interval with a better surface finish while improving the cutting edge lifetime.

The proposed damping mechanism might be applied to any other beam shaped tools and structures. Because of flexible shape and mechanism, the use of the proposed frictional damper is not limited to circular rotating [44, 45] or solid sections [43, 46, 47] but can also be applied to any type of sections under different conditions. It can also be used for vibration reduction in flat-shaped and hollow structures such as robot links and turbine blades. In order to boost the effectiveness of the proposed mechanism, the contact surfaces may be increased by threading them or using multi-layered pins like the one used by Madoliat et al. [46, 47].

Author contribution Conception and design of study, construction of the analytical model, revising the manuscript critically for important

intellectual content, and approval of the version of the manuscript to be published: Sajad Hayati. Sample fabrication, performing the experimental tests, analysis and/or interpretation of data, and drafting the manuscript: Mehdi Shahrokh. FEM analysis, analytical study, and drafting the manuscript: Ali Hedayati.

Declarations

Ethics approval Not applicable

Consent to participate Not applicable

Consent for publication Not applicable

Conflict of interest The authors declare no competing interests.

References

- Siddhpura M, Paurobally R (2012) A review of chatter vibration research in turning. *Int J Mach Tools Manuf* 61:27–47. <https://doi.org/10.1016/j.ijmactools.2012.05.007>
- Munoa J, Beudaert X, Dombovari Z, Altintas Y, Budak E, Brecher C, Stepan G (2016) Chatter suppression techniques in metal cutting. *CIRP Ann* 65(2):785–808. <https://doi.org/10.1016/j.cirp.2016.06.004>
- Yue C, Gao H, Liu X, Liang SY, Wang L (2019) A review of chatter vibration research in milling. *Chin J Aeronaut* 32(2):215–242. <https://doi.org/10.1016/j.cja.2018.11.007>
- Vasanth XA, Paul PS, Lawrance G, Varadarajan AS (2019) Vibration control techniques during turning process: a review. *Aust J Mech Eng*:1–21. <https://doi.org/10.1080/14484846.2019.1585224>
- Yang F, Zhang B, Yu J (2003) Chatter suppression with multiple time-varying parameters in turning. *J Mater Process Technol* 141(3):431–438. [https://doi.org/10.1016/S0924-0136\(03\)00427-8](https://doi.org/10.1016/S0924-0136(03)00427-8)
- Yusoff AR, Sims ND (2011) Optimisation of variable helix tool geometry for regenerative chatter mitigation. *Int J Mach Tools Manuf* 51(2):133–141. <https://doi.org/10.1016/j.ijmactools.2010.10.004>
- Comak A, Budak E (2017) Modeling dynamics and stability of variable pitch and helix milling tools for development of a design method to maximize chatter stability. *Precis Eng* 47:459–468. <https://doi.org/10.1016/j.precisioneng.2016.09.021>
- Lin C-Y, Yeh S-S (2020) Integration of cutting force control and chatter suppression control into automatic cutting feed adjustment system design. *Mach Sci Technol* 24(1):65–95. <https://doi.org/10.1080/10910344.2019.1636265>
- Otto A, Radons G (2013) Application of spindle speed variation for chatter suppression in turning. *CIRP J Manuf Sci Technol* 6(2):102–109. <https://doi.org/10.1016/j.cirpj.2013.02.002>
- Shamoto E, Mori T, Sencer B, Suzuki N, Hino R (2013) Suppression of regenerative chatter vibration in multiple milling utilizing speed difference method – analysis of double-sided milling and its generalization to multiple milling operations. *Precis Eng* 37(3):580–589. <https://doi.org/10.1016/j.precisioneng.2013.01.003>
- Yamato S, Ito T, Matsuzaki H, Kakinuma Y (2018) Programmable optimal design of sinusoidal spindle speed variation for regenerative chatter suppression. *Procedia Manuf* 18:152–160. <https://doi.org/10.1016/j.promfg.2018.11.020>
- Wang C, Zhang X, Yan R, Chen X, Cao H (2019) Multi harmonic spindle speed variation for milling chatter suppression and

- parameters optimization. *Precis Eng* 55:268–274. <https://doi.org/10.1016/j.precisioneng.2018.09.017>
13. Petrakov Y (2019) Chatter suppression technologies for metal cutting. *Mech Adv Technol* 2(86):51–60. <https://doi.org/10.20535/2521-1943.2019.86.185849>
 14. Gienke O, Pan Z, Yuan L, Lepper T, Van Duin S (2019) Mode coupling chatter prediction and avoidance in robotic machining process. *Int J Adv Manuf Technol* 104(5):2103–2116. <https://doi.org/10.1007/s00170-019-04053-x>
 15. Albertelli P, Musletti S, Leonesio M, Bianchi G, Monno M (2012) Spindle speed variation in turning: technological effectiveness and applicability to real industrial cases. *Int J Adv Manuf Technol* 62(1):59–67. <https://doi.org/10.1007/s00170-011-3790-8>
 16. Albertelli P, Mussi V, Ravasio C, Monno M (2012) An experimental investigation of the effects of spindle speed variation on tool wear in turning. *Procedia CIRP* 4:29–34. <https://doi.org/10.1016/j.procir.2012.10.006>
 17. Salles L, Scippa A, Grossi N, Campatelli G (2016) Investigating actuation strategies in active fixtures for chatter suppression. *Procedia CIRP* 46:311–314. <https://doi.org/10.1016/j.procir.2016.04.073>
 18. Salles L, Grossi N, Tsalhalis J, Scippa A, Campatelli G (2016) Intelligent fixtures for active chatter control in milling. *Procedia CIRP* 55:176–181. <https://doi.org/10.1016/j.procir.2016.08.019>
 19. Munoa J, Mancisidor I, Loix N, Uriarte LG, Barcena R, Zatarain M (2013) Chatter suppression in ram type travelling column milling machines using a biaxial inertial actuator. *CIRP Ann* 62(1):407–410. <https://doi.org/10.1016/j.cirp.2013.03.143>
 20. Dohner JL, Lauffer JP, Hinnerichs TD, Shankar N, Regelbrugge M, Kwan C-M, Xu R, Winterbauer B, Bridger K (2004) Mitigation of chatter instabilities in milling by active structural control. *J Sound Vib* 269(1):197–211. [https://doi.org/10.1016/S0022-460X\(03\)00069-5](https://doi.org/10.1016/S0022-460X(03)00069-5)
 21. Li D, Cao H, Zhang X, Chen X, Yan R (2019) Model predictive control based active chatter control in milling process. *Mech Syst Signal Process* 128:266–281. <https://doi.org/10.1016/j.ymssp.2019.03.047>
 22. Zhang X, Wang C, Liu J, Yan R, Cao H, Chen X (2019) Robust active control based milling chatter suppression with perturbation model via piezoelectric stack actuators. *Mech Syst Signal Process* 120:808–835. <https://doi.org/10.1016/j.ymssp.2018.10.043>
 23. Moradian H, Abbasi MH, Moradi H (2020) Adaptive sliding mode control of regenerative chatter and stability improvement in boring manufacturing process with model uncertainties. *Proc Inst Mech Eng C J Mech Eng Sci* 234(6):1171–1181
 24. Wan S, Li X, Su W, Yuan J, Hong J, Jin X (2019) Active damping of milling chatter vibration via a novel spindle system with an integrated electromagnetic actuator. *Precis Eng* 57:203–210. <https://doi.org/10.1016/j.precisioneng.2019.04.007>
 25. Alammari Y, Sanati M, Freiheit T, Park SS (2015) Investigation of boring bar dynamics for chatter suppression. *Procedia Manuf* 1:768–778. <https://doi.org/10.1016/j.promfg.2015.09.059>
 26. Hayati S, Hajaliakbari M, Rajabi Y, Rasaei S (2017) Chatter reduction in slender boring bar via a tunable holder with variable mass and stiffness. *Proc Inst Mech Eng B J Eng Manuf* 232(12):2098–2108. <https://doi.org/10.1177/0954405417690554>
 27. Burtscher J, Fleischer J (2017) Adaptive tuned mass damper with variable mass for chatter avoidance. *CIRP Ann* 66(1):397–400. <https://doi.org/10.1016/j.cirp.2017.04.059>
 28. Wang C, Zhang X, Liu Y, Cao H, Chen X (2018) Stiffness variation method for milling chatter suppression via piezoelectric stack actuators. *Int J Mach Tools Manuf* 124:53–66. <https://doi.org/10.1016/j.ijmactools.2017.10.002>
 29. Li D, Cao H, Liu J, Zhang X, Chen X (2019) Milling chatter control based on asymmetric stiffness. *Int J Mach Tools Manuf* 147:103458. <https://doi.org/10.1016/j.ijmactools.2019.103458>
 30. Tang B, Akbari H, Pouya M, Pashaki PV (2019) Application of piezoelectric patches for chatter suppression in machining processes. *Measurement* 138:225–231. <https://doi.org/10.1016/j.measurement.2019.02.003>
 31. Mei D, Kong T, Shih AJ, Chen Z (2009) Magnetorheological fluid-controlled boring bar for chatter suppression. *J Mater Process Technol* 209(4):1861–1870. <https://doi.org/10.1016/j.jmatprotec.2008.04.037>
 32. Biju CV, Shunmugam MS (2019) Performance of magnetorheological fluid based tunable frequency boring bar in chatter control. *Measurement* 140:407–415. <https://doi.org/10.1016/j.measurement.2019.03.073>
 33. Ema S, Marui E (2000) Suppression of chatter vibration of boring tools using impact dampers. *Int J Mach Tool Manu* 40:1141–1156. [https://doi.org/10.1016/S0890-6955\(99\)00119-4](https://doi.org/10.1016/S0890-6955(99)00119-4)
 34. Miguélez MH, Rubio L, Loya JA, Fernández-Sáez J (2010) Improvement of chatter stability in boring operations with passive vibration absorbers. *Int J Mech Sci* 52(10):1376–1384. <https://doi.org/10.1016/j.ijmecsci.2010.07.003>
 35. Yang Y, Muñoz J, Altintas Y (2010) Optimization of multiple tuned mass dampers to suppress machine tool chatter. *Int J Mach Tools Manuf* 50(9):834–842. <https://doi.org/10.1016/j.ijmactools.2010.04.011>
 36. Rubio L, Loya JA, Miguélez MH, Fernández-Sáez J (2013) Optimization of passive vibration absorbers to reduce chatter in boring. *Mech Syst Signal Process* 41(1):691–704. <https://doi.org/10.1016/j.ymssp.2013.07.019>
 37. Bansal A, Law M (2018) A receptance coupling approach to optimally tune and place absorbers on boring bars for chatter suppression. *Procedia CIRP* 77:167–170. <https://doi.org/10.1016/j.procir.2018.08.267>
 38. Yadav A, Talaviya D, Bansal A, Law M (2020) Design of chatter-resistant damped boring bars using a receptance coupling approach. *J Manuf Mater Process* 4(2):53
 39. da Silva MM, Venter GS, Varoto PS, Coelho RT (2015) Experimental results on chatter reduction in turning through embedded piezoelectric material and passive shunt circuits. *Mechatronics* 29:78–85. <https://doi.org/10.1016/j.mechatronics.2015.06.002>
 40. Yigit U, Cigeroglu E, Budak E (2017) Chatter reduction in boring process by using piezoelectric shunt damping with experimental verification. *Mech Syst Signal Process* 94:312–321. <https://doi.org/10.1016/j.ymssp.2017.02.044>
 41. Zhang Z, Li H, Meng G, Ren S (2017) Milling chatter suppression in viscous fluid: a feasibility study. *Int J Mach Tools Manuf* 120:20–26. <https://doi.org/10.1016/j.ijmactools.2017.02.005>
 42. Portentos M, Pennacchi P, Chatterton S (2017) Comparison of the dynamic response of two columns of milling machines made of standard carpentry and metal foam sandwiches. *J Vib Control* 23(17):2782–2794. <https://doi.org/10.1177/1077546315622355>
 43. Marui E, Ema S, Hashimoto M, Wakasawa Y (1998) Plate insertion as a means to improve the damping capacity of a cutting tool system. *Int J Mach Tools Manuf* 38(10):1209–1220. [https://doi.org/10.1016/S0890-6955\(98\)00001-7](https://doi.org/10.1016/S0890-6955(98)00001-7)
 44. Kim NH, Won D, Ziegert JC (2006) Numerical analysis and parameter study of a mechanical damper for use in long slender endmills. *Int J Mach Tools Manuf* 46(5):500–507. <https://doi.org/10.1016/j.ijmactools.2005.07.004>
 45. Ziegert JC, Stanislaus C, Schmitz TL (2006) Enhanced damping in long slender end mills. *J Manuf Process* 8(1):39–46
 46. Madoliat R, Hayati S, Ghalebahman AG (2011) Modeling and analysis of frictional damper effect on chatter suppression in a Slender Endmill Tool. *J Adv Mech Des Syst Manuf* 5(2):115–128
 47. Madoliat R, Hayati S, Ghasemi Ghalebahman A (2011) Investigation of chatter suppression in slender endmill via a

- frictional damper. *Sci Iran* 18(5):1069–1077. <https://doi.org/10.1016/j.scient.2011.08.008>
48. Moetakef-Imani B, Yusefian NZ (2009) Dynamic simulation of boring process. *Int J Mach Tools Manuf* 49(14):1096–1103. <https://doi.org/10.1016/j.ijmachtools.2009.07.008>
49. Tlustý J (1986) Dynamics of high-speed milling. *J Eng Ind* 108(2): 59–67. <https://doi.org/10.1115/1.3187052>
50. Tlustý J (1985) Machine dynamics. In: King RI (ed) *Handbook of high speed machining technology*. Chapman and Hall, New York, pp 48–153
51. Quintana G, Ciurana J (2011) Chatter in machining processes: a review. *Int J Mach Tools Manuf* 51(5):363–376. <https://doi.org/10.1016/j.ijmachtools.2011.01.001>

Publisher's note Springer Nature remains neutral with regard to jurisdictional claims in published maps and institutional affiliations.